Technical Sciences
Academy of Romania
www.jesi.astr.ro

Journal of Engineering Sciences and Innovation
Volume 8, Issue 4 / 2023, pp. 363 - 372
http://doi.org/10.56958/jesi.2023.8.4.363

C. Chemical Engineering, Materials Science and Engineering

*Received **24 July 2023*** *Accepted **4 December 2023***
*Received in revised form **17 October 2023***

Oxidation of a conventionally cast Cantor high entropy alloy in an argon flow during creep tests at high temperature

PATRICE BERTHOD[1,2*]

[1]Faculté des Sciences et Technologies, Université de Lorraine, Campus Victor Grignard, 54500 Vandoeuvre–lès–Nancy, France
[2]Institut Jean Lamour, Université de Lorraine, Campus Artem, 2 allée André Guinier, 54000 Nancy, France

Abstract. A conventionally cast version of the Cantor alloy (equimolar in Co, Ni Fe, Mn and Cr) was elaborated and samples were cut to carry out three points flexural creep tests according to a (1000, 1050, 1100°C) × (10, 20 and 30 MPa) array to explore the possibility of use in term of temperature and stress. For a majority of cases the deformation rates were too high, revealing a lack of practical interest, except for 10 MPa for which, whatever the temperature tests longer than 100 hours were realized. These tests were all performed under a slow flow of argon o preserve the alloy from oxidation during the tests. In fact, oxygen present as impurity (about 10 ppm) induced a signification oxidation of the samples which were covered by complex oxides involving Mn and Cr in various proportions and for different stoichiometries for the oxygen importance point of view, with thickness not far from what can be obtained in synthetic air for similar conditions.

Keywords: Cantor alloy, High temperature creep test, Argon flow, Oxidation, Electron microscopy.

Introduction

Among the now rather broad variety of existing high entropy alloys (HEAs) [1], the Cantor's alloy keeps a particular place since it is one of the earliest alloys of this category to appear [2,3]. Till today it has been synthesized, as bulk materials or coatings, following various elaboration techniques [3–5]. Many properties of this CoNiFeMnCr alloys and numerous derivative alloys are now well known, except the ones at the temperature levels of superalloys service, i.e. T ≥ 1000°C [7, 8].

*Correspondence address: patrice.berthod@univ-lorraine.fr

Notably, The Cantor alloy presents a high melting point [9,10] which allows envisaging to use it at elevated temperatures (1200 °C and more). Curiously creep results obtained for the Cantor alloy are rare and limited to not so high temperatures, for instance 800°C [11] or 980°C [12]. 1000°C and more seem to be not considered for exploring the creep behavior of this alloy, despite its existence since 2004 [3]. This became the initial objective of the present work in which the resistance against creep was investigated for several combinations of temperature and stress, for a 3 points flexural loading mode. In parallel the oxidized states of the samples were characterized to approximately specify the oxide development over their surfaces and the induced chemical change in the outermost layers of alloy.

Methodology

The Cantor alloy destined to this work was elaborated by classical foundry under argon. Parts of pure elements (Alfa Aesar, purity higher than 99.9%) were carefully weighed to obtained the masses of Co, Ni, Fe, Mn and Cr allowing the equimolar character of the alloy (20 at.% for each of the five elements, total mass: 40g). These parts were placed in the segmented copper crucible of a high frequency induction furnace (CELES, France). The chamber was closed by placing a silica tube around the crucible and a copper coil was placed around the silica tube and the crucible. After three {pumping to primary vacuum, pure Ar introduction} cycles, the internal atmosphere was rated to 300 millibars of pure argon. An alternative current with a 100 kHz frequency and a 5kV voltage was applied increasingly, inducing Foucault's currents which heated by Joule effect the external faces of the introduced metallic parts. After about 2 minutes all metals were melted and the obtained liquid alloy was maintained at maximal power during ten minutes to achieve complete chemical homogenization. By decreasing power, the alloys cooled in the liquid state, solidified and cooled in the solid state.

The obtained ovoid ingot was immersed in a molten cold {resin + hardener} mixture which rigidified during the following four hours. After extraction out of the plastic mold, it was cut using a precision metallographic saw, rather easily thanks to the cylindrical geometry of the embedded ingot. A series of parallelepipeds with $2 \times 1 \times 15$ mm^3 dimensions (with × thickness × length) were cut, again with the precision saw which gave good surface states to all faces of these samples.

Each sample, the dimensions of which were accurately measured, was placed in a SETARAM 92-16.18 dilatometer adapted to allow performing creep bending tests. The two bottom supports, spaced by 12 mm, were alumina cylinders and the third (top) support, placed in the middle was connected to a sensor able to accurately measure the central deformation of the samples during the creep tests. The load to apply through the central top support was calculated taking into account the exact width and thickness of the sample to produce the desired maximal tensile stress in the middle of the bottom of the sample. The heating to the stage temperature was

carried out at 20°C / minute, the maximal time duration of the isothermal part of the test was initially chosen equal to 150 hours. This isothermal stage was, in some cases, shortened in case of rapid deformation until contact of the sample with the basis of the alumina lower floor. In such case the deformation curve plotted versus time became globally horizontal, with a. 1.1 to 1.2 mm deformation, value depending of the thickness of the sample. The final cooling was achieved at -20°C / minute. Prior to heating, the load was progressively applied until reaching the value targeted for the constant load. The load was removed after complete post–test cooling. All along the thermal cycle the sample was exposed to a 2L/h continuous flow of pure argon (containing oxygen impurities, about 10 ppm). The diameter of the tubular chamber containing the sample which was crossed by the argon flow was 18 mm. The linear rate of Ar was thus about 1.6 mm/s). A photograph of the sample positioned in the total alumina device before closing the chamber, and a descriptive scheme of the solicitation mode are given in Figure 1. The temperatures chosen for the tests were 1000°C, 1050°C and 1100°C, and for each temperature three stresses to be continuously applied were rated by adjusting the applied load versus the exact transversal dimensions of the sample: 10 MPa, 20 MPa and 30 MPa.

The curves, which were progressively plotted on the screen during the tests, were plotted in a spreadsheet and analyzed. The crept specimens, more or less deformed at the end of experiment, depending on the temperature and load values, were also more or less oxidized by the flow of oxygen impurities. They were embedded in resin, and ground (SiC papers from 240 grade to 1200 grade) and polished (micrometric alumina particles on a textile disk) to achieve a mirror–like state for the obtained metallographic samples. The fractography and oxidation states of these samples were characterized with observation (back scattered electrons imaging, BSE) and Energy Dispersion Spectrometry analysis (EDS) with a scanning electron microscope (SEM). This one was a JEOL JSM-6010LA one.

Results and Discussion

Initial chemical and microstructure controls of the studied alloy

The chemical composition measured by several full frame EDS analyses on the metallographic sample containing the as–cast part of the alloy evidenced that the targeted composition was successfully obtained. The microstructure was examined at several magnifications and in different locations randomly selected. The alloy is single phased and no problems of heterogeneity such as not melted elements was encountered.

Behavior of the alloy in 3 points flexural creep

Nine deformation curves were obtained, corresponding to the nine {1000, 1050 and 1100°C} × {10 MPa, 20 MPa and 30 MPa} sets of test conditions. They can be

described by Figure 2. Many of them present a more or less fast deformation and an horizontal stage after only several tens hours, this indicating the contact with the alumina bottom (case of the {1000°C, 20 MPa} and {1000°C, 30 MPa} curves in Figure 2). Several ones, in contrast, demonstrated a much lower deformation rate (illustrated by the {1000°C, 10 MPa} curve in Figure 2), and it was decided to stop the test after more or less 150 hours in absence of any sign suggesting an acceleration of the deformation.

As this can be seen in the recapitulative Table 1, all the tests carried out with 20 MPa or 30 MPa as induced maximal tensile stress led to fast deformation and contact with the alumina basis after less than 100h (1000°C), less than 50h (1050°C) and even less than 10h (1100°C). Only the tests performed for 10 MPa led to low deformation rates, this leading to stop them after more than 100 hours during the steady state part of creep. At such high level of temperature, the Cantor alloy cannot be used in service for high or moderate loading. Only 10 MPa and lower stress can be applied for preserving acceptable creep resistance.

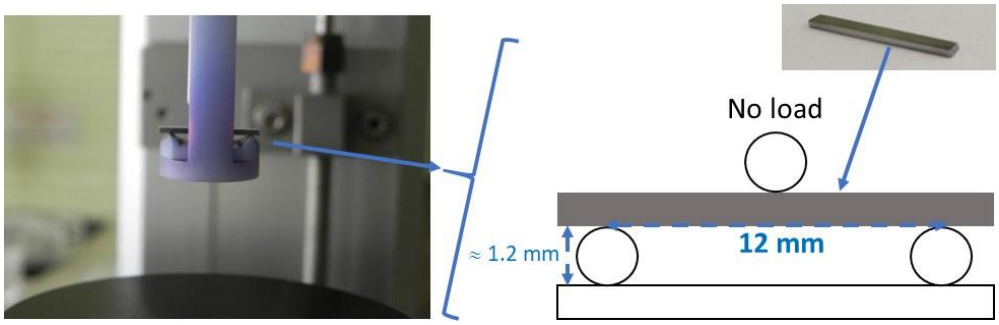

Fig. 1. Photograph of the sample positioned in the alumina device taken prior to chamber clsing (left) and principle of the three points flexural test before applying the load (right).

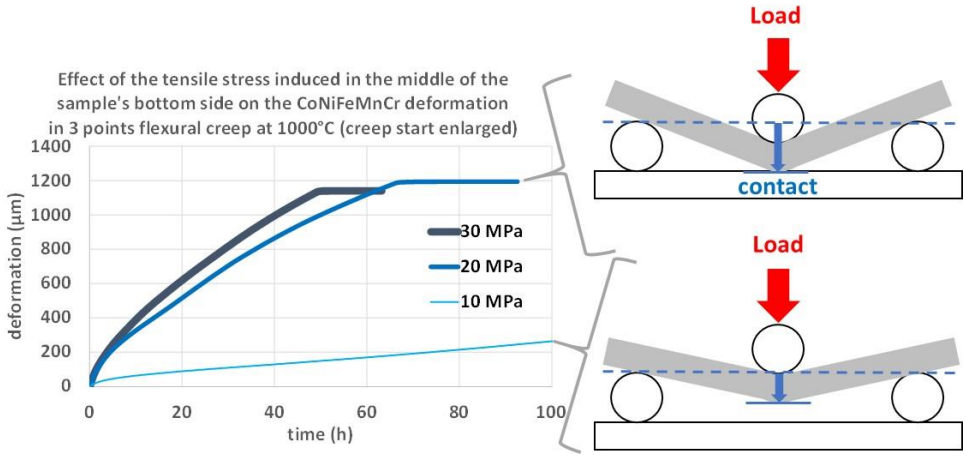

Fig. 2. Photograph of the sample positioned in the alumina device taken prior to chamber clsing (left) and principle of the three points flexural test before applying the load (right).

The examination of the metallographic samples prepared with the crept specimens allowed observing the propagation of a more or less great number of cracks with various degrees of progress. These observations are summarized in Figure 3 in which the crack progress is illustrated versus both temperature and duration of test. This allows first observing the fissuration state

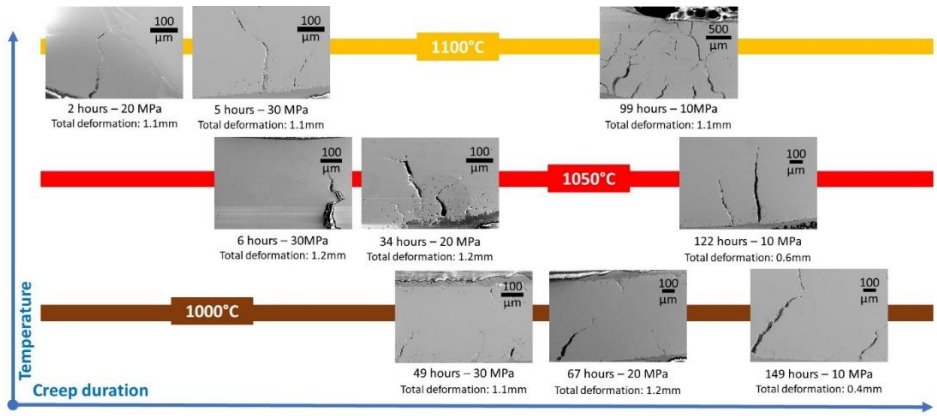

Fig. 3. Scheme and photographs summarizing the progression of the multiple cracks versus the tests conditions (temperature and duration of test).

Behavior of the alloy oxidation in atmosphere very poor in oxygen

Between the contact with the alumina basis and the anticipated end of the test, the crept samples were exposed to the argon flow during the times given in the last column of Table 2. These durations are higher than the {deformation to contact} ones, in contrast with the three {10 MPa} tests for which test durations and durations of exposure to argon are the same. All samples were obviously covered by oxides which formed during the tests. The importance of the oxides formed, increasing with temperature and with exposure time, is illustrated in Figure 4.

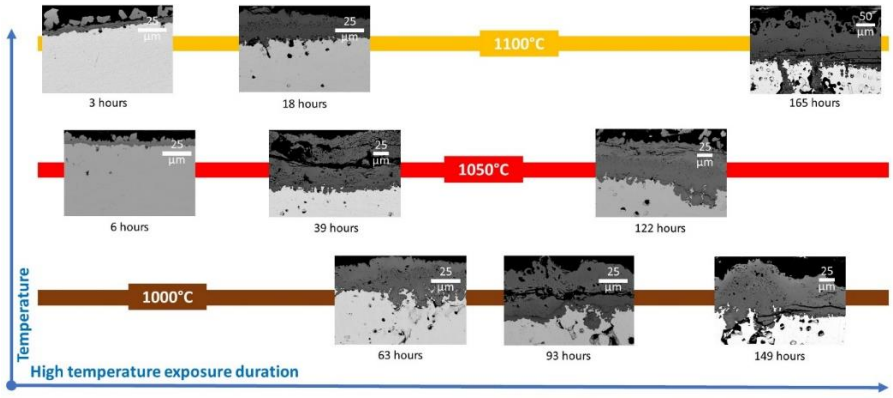

Fig. 4. Scheme and photographs summarizing the growth of the external oxide scales versus the tests conditions (temperature and duration of exposure ≥ duration of creep test).

The average thickness of the estimated for each sample using imaging in BSE mode with the SEM is represented versus temperature and time in Figure 5. The oxide scale thickness ranges from 25 µm (63h) to 50 µm (149h), from 5 µm (6h) to 60 µm (122h) and from 5 µm (3h) to 150 µm (165h), for 1000°C, 1050°C and 1100°C respectively.

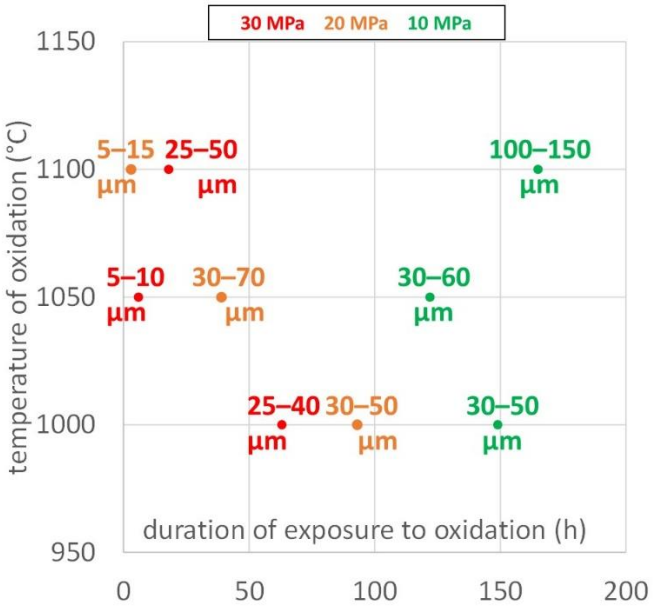

Fig. 5. Evolution of the ranges of oxide scale thickness with temperature and exposure duration.

These oxides scales formed in a flow of atmosphere very poor in oxygen (10 ppm O_2 in Ar, 1 atm) are thus sensibly as thick as after oxidation in 80%N_2-20%O_2 (about 25 µm for 50h [13] and 50 µm for 50h [14]).

The oxides externally formed and the alloy sub–surfaces were subjected to EDS elemental mapping (1000°C during 63, 93 and 149 hours in Figure 6, 1050°C during 6, 39 and 122 hours in Figure 7, 1100°C during 3, 18 and 165 hours in Figure 8). These X–maps evidence that the metals constituting the alloys which are involved in the oxidation phenomenon are mainly (almost exclusively) manganese and chromium. Mn seems present in high concentration everywhere in the oxide scale while chromium tends to be concentrated in the part of the scale which is the closest to the alloy. In the subsurface the impoverishment in both Mn and Cr (more extended for Mn than for Cr) is clearly visible.

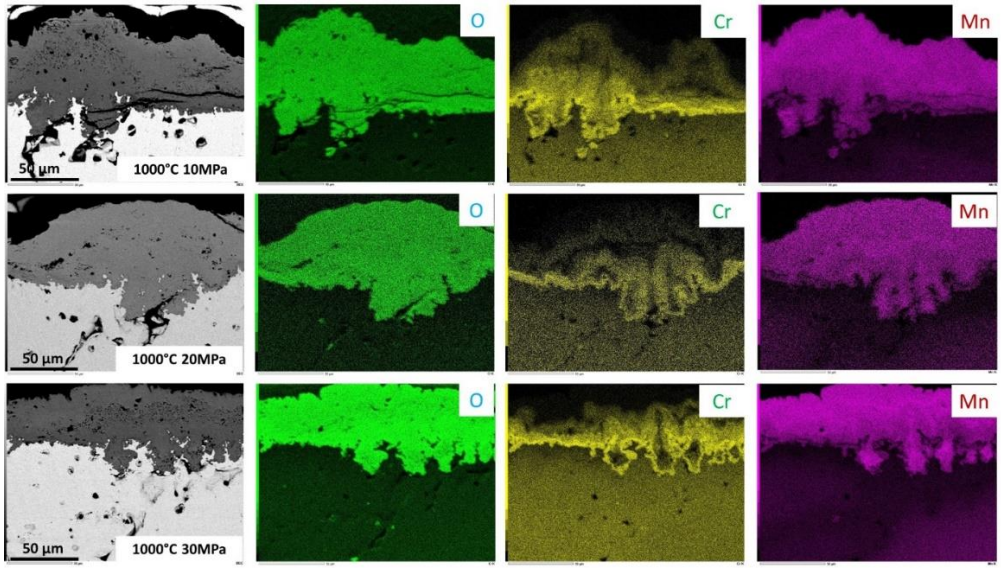

Fig. 6. EDS elemental mapping of the oxide scale and sub–surface of the samples oxidized during 63, 93 and 149h at 1000°C (crept under 30, 20 and 10 MPa respectively).

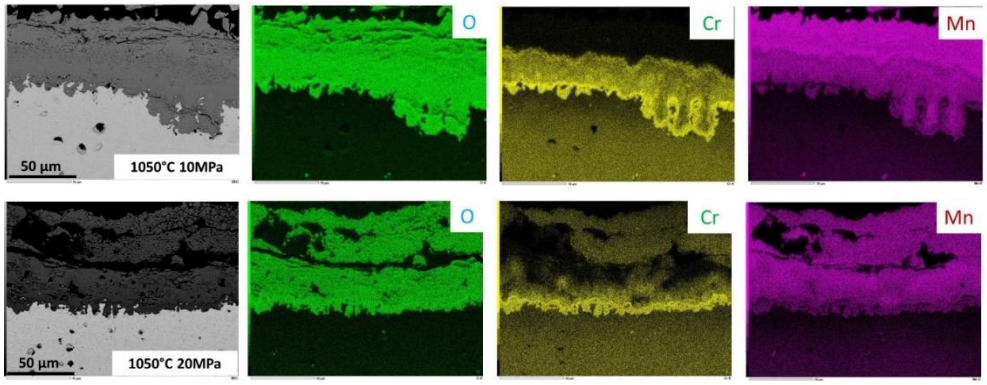

Fig. 7. EDS elemental mapping of the oxide scale and sub–surface of the samples oxidized during 39 and 122h at 1050°C (crept under 20 and 10 MPa respectively; the one crept under 30MPa presented too thin oxide scale to perform interesting EDS X–map).

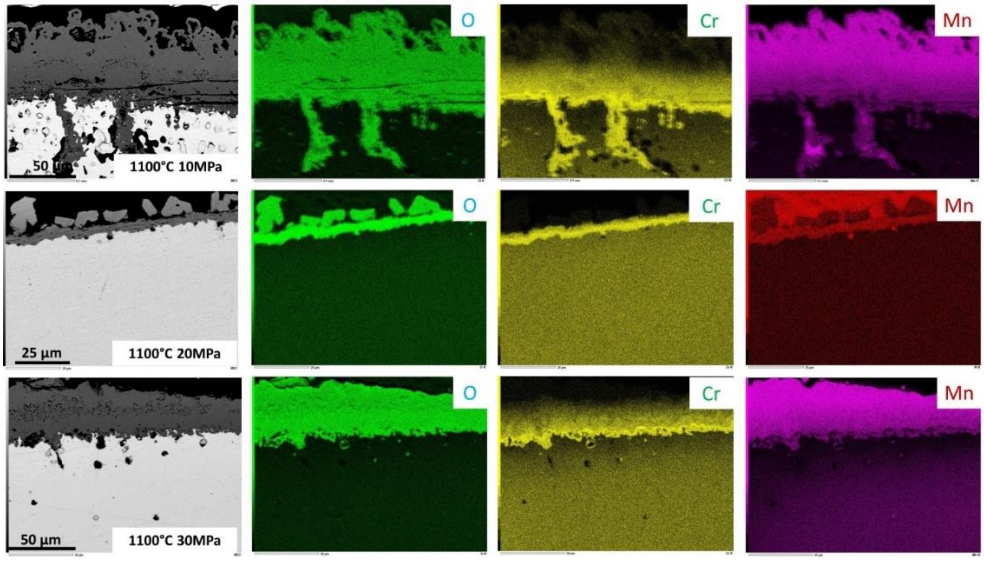

Fig. 8. EDS elemental mapping of the oxide scale and sub–surface of the samples oxidized during 18, 3 and 165h at 1100°C (crept under 30, 20 and 10 MPa respectively).

The oxides were specified by performing a series of EDS spot analysis per oxide type seen in each crept sample. The results are summarized in Figure 9 which evidenced the great complexity of constitution of the scale. All samples, at least which were exposed to the argon flow several tens hours, are covered by oxides of numerous types: manganese oxides (MnO_2, Mn_2O_3 and/or MnO) mainly in the outermost part of the scale, complex oxides of both manganese and chromium ($(Mn, Cr)O_2$, $(Mn,Cr)_2O_3$ with various Mn and Cr proportions) everywhere and in some cases chromium oxides (Chromia: Cr_2O_3) at the interface of the scale and the alloy. The mixed oxide involving both Mn and Cr tend to be richer in Mn than in Cr in the more external part of the scale, and to be richer in Cr than in Mn in the most internal part of this scale. The importance of oxygen in the stoichiometry becomes higher and higher from the interface with the alloy to the interface with air. This is true for the oxides of manganese as well as for the mixed oxides of both Mn and Cr.

The formation of oxides of Mn and Cr induced an impoverishment in these two elements in the sub – surface of the alloy, as visualized by the EDS X–maps (Figures 6, 7 and 8), and which can start to be quantified by simply performing EDS spot analysis in the alloy close and along the alloy/scale interface.

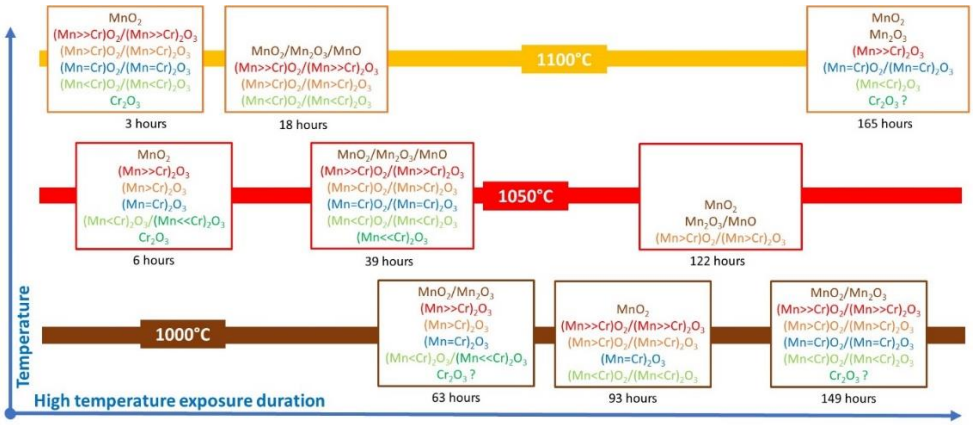

Fig. 9. Constitution of the external oxide scale versus temperature and exposure duration.

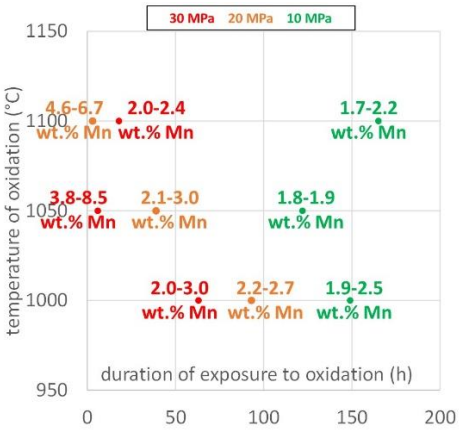

Fig. 10. Evolution with temperature and exposure duration of the ranges of the manganese contents in alloy very close to the interface with oxide scale (several EDS spot analyses).

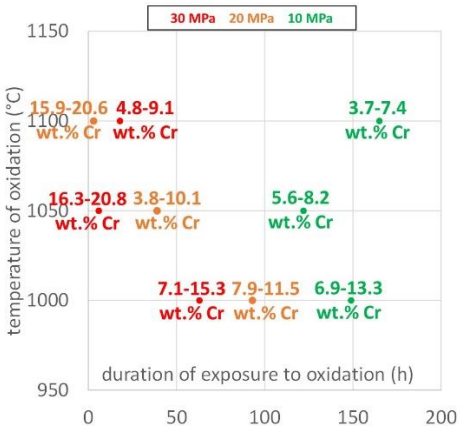

Fig. 11. Evolution with temperature and exposure duration of the ranges of the chromium contents in alloy very close to the interface with oxide scale (several EDS spot analyses).

From Figure 10 which represents the evolution of the sub–surface Mn content (very close to the interface with the oxide scale) with temperature and the duration of high temperature exposure to the argon flow, one can state that the Mn content, initially of about 20 wt.% Mn, has considerably decreased, down to a very low value which decreases with both temperature and oxidation duration from 2.0–3.0 wt.% Mn (1000°C, 63 hours) to 1.7–2.2 wt.% (1100°C, 165 hours). This is the same trend versus temperature and duration for the chromium content in sub–surface very close to the interface with the scale (Figure 11): it decreases from about 20 wt.%Cr to 7–15 wt.%Cr (1000°C, 63h) to 4–7 wt.%Cr (1100°C, 165h). These Cr contents in sub – surface are higher than the Mn contents but lower than the values generally considered for nickel–based and cobalt–based superalloys as critical to stay chromia–forming and thus very resistant against hot oxidation. This is thus not surprising that chromia is not the single oxide to form, and furthermore,

in contrast, rather the minor oxide to form (by comparison with the Mn oxides and (Mn,Cr) oxides).

Conclusion

These flexural creep tests clearly demonstrated that the Cantor alloy in classically cast condition is not performing at temperatures as high as 1000°C and beyond, globally. The performances for loads inducing 30 MPa or 20 MPa as tensile stresses are not satisfying for reasonably long durations. This is only for 10 MPa as induced tensile stress that this alloy is possibly suitable for long–term service. This seems true for all the test temperatures: the alloy is more sensitive to stress than to temperature.

These tests also showed that this alloy is also sensitive to oxidation in atmospheres very poor in oxygen when oxygen is constantly renewed as this was the case for the {10 ppm O_2}–containing argon flow although argon was expected to protect it against oxidation. Furthermore, the oxidation rate appeared to be not considerably slower than in a flow of synthetic air which contains 20% O_2. This suggests that using an inert atmosphere which necessary contains impurities including oxygen is not an adequate solution to perform, on the equimolar CoNiFeMnCr alloy, high temperature creep tests decoupled from oxidation. Vacuum can be experimented.

Acknowledgments

The author wishes to thank Mr. Lionel Aranda for his technical help performing the creep runs.

References

[1] Ye Y.F., Wang Q., Lu J., Liu C.T., Yang Y., *Materials Today*, **19**, 349, 2016.
[2] Cantor B., *Progress in Materials Science*, **120**, 100754, 2021. https://doi.org/10.1016/j.pmatsci.2020.100754
[3] Xu D., Wang, M., Li T., Wei X., Lu Y., *Microstructures*, **2**, 2022001, 2022, https://dx.doi.org/10.20517/microstructures.2021.10
[4] Kawamura M., Asakura M., Okamoto N. L., Kishida K., Inui H., George E.P, *Acta Materialia*, **203**, 116454, 2021.
[5] Osintsev K., Konovalov S., Zaguliaev D., Ivanov Y., Gromov V., Panchenko I., *Metals*, **12**, 197, 2022.
[6] Hu M., Cao Q.P., Wang X.D., Zhang D.X., Jiang J.Z., *Metals*, **12**, 197, 2022.
[7] Sims C.T., Stoloff N.S., Hagel W.C., *Superalloys II. High Temperature Materials for Aerospace and Industrial Power*, John Wiley & Sons, 1987.
[8] Donachie M.J., Donachie S.J.; *Superalloys: A Technical Guide* (2nd edition), ASM International, 2002.
[9] Zhang X., Ye H., Huang J.C., Liu T., Lin P., Wu Y., Tsai M., Liao Y., Jang J.S.C., *Materials*, **13**, 36, 2020. doi:10.3390/ma13010036
[10] Tsai M., Huang J., Lin P., Liu T., Liao Y., Jang J.S., Song S., Nieh T., *Intermetallics*, **103**, 88, 2018.
[11] Chen S., Qiao J., Diao H., Yang T., Poplawsky J., Li W., Meng F., Tong Y., Jiang L., Liaw P.K., Gao Y, *Acta Materialia*, **244**,118600, 2023.
[12] Glatzel U., Schleifer F., Gadelmeier C., Krieg F., Müller M., Mosbacher M., Völkl R., *Metals* **11**, 1130, 2021. https://doi.org/10.3390/met11071130
[13] Berthod P., *Materials and Corrosion*, **74**, 1312, 2023. https://doi.org/10.1002/maco.202213721
[14] Berthod P., *High Temperature Corrosion of Materials*, **100**, 177, 2023